International Journal of Material Forming (2023) 16:60
https://doi.org/10.1007/s12289-023-01781-0

ORIGINAL RESEARCH

Investigation of feature-based and space-filling tool path strategies for formability in incremental sheet metal forming

Sahil Bharti[1] · Karthik Subramanya Karvaje[1] · Hariharan Krishnaswamy[1] · Anupam Agrawal[2] · S. K. Panigrahi[1]

Received: 13 June 2023 / Accepted: 10 August 2023 / Published online: 15 September 2023
© The Author(s), under exclusive licence to Springer-Verlag France SAS, part of Springer Nature 2023

Abstract

Incremental sheet metal forming (ISF) is a versatile dieless forming process for manufacturing complex sheet metal components. The toolpath is one of the most critical process parameters, significantly influencing the ISF formability. The conventional toolpath strategies, such as spiral and constant z-slice-based tool paths, do not prove helpful for complex asymmetries in part geometry. The approach to toolpath planning in ISF should consider both material behavior and design complexity. This work compares conventional toolpaths with two strategies, namely feature-based and space-filling fractal tool paths. Material thinning and geometric deviations are critical limitations for successful part development. All toolpath strategies were evaluated for material distribution, geometric accuracy, and fracture depth using four carefully designed components with gradually increasing asymmetry. As evident from the results obtained, the material deformation was sensitive to the choice of toolpath strategies. The feature-based tool path captures the part curvatures more uniformly, leading to homogeneous thickness distribution. At the same time, fractal-based strategies lead to lower overall geometric deviation in the region of curved profiles.

Keywords Incremental sheet metal forming (ISF) · Fractal toolpath · Feature-based toolpath

Introduction

Incremental sheet metal forming (ISF) is a die-less forming technique characterized by the progressive local deformation imposed across a sheet metal along a predefined tool path. Forgoing the need for form dies simplifies the tooling, enabling quick customization in part design for functional sheet metal components.

It is widely established that the formability in ISF is considerably higher than a conventional stamping process [1]. The dynamic tool-sheet contact serves to prevent the occurrence of strain localization and effectively delays the formation of local necks. However, progressive stretching of the material by the tool gradually thins the material resulting in a fracture. The limiting strains measured at fracture are considerably greater in magnitude in comparison to the strains observed at local necks [2]. As a result, the fracture forming limit (FFL) line is preferred to represent formability limits in ISF instead of necking limits [3].

Extensive research has been conducted on the influence of several process parameters, such as material ductility, sheet thickness, tool radius, and forming speed, on formability in ISF [4–6]. The forming angle parameter, alternatively referred to as the draw angle, is a useful metric that directly indicates the ISF formability. Bhattacharya et al. [4] and Silva et al. [7] proposed an empirical relation correlating the formability to the sheet thickness and tool radius. The high-speed formability of aluminum and steel alloys was investigated by Abbrigio et al. [5] and Vanhove et al. [6] for developing asymmetric components. They observed that aluminum 1050 appeared insensitive, while aluminum 5xxx series favored high-speed forming with feed rates of 600 m/min due to the diminished Portevin-Le Chatelier effect. In contrast, strain-rate-sensitive materials such as (DP600, DP780) dual-phase steels exhibited reduced formability at higher speeds due to higher strain rate hardening. The local impositions of deformations in ISF necessitate the consideration of tool shape

✉ Sahil Bharti
sahibhart@gmail.com

Hariharan Krishnaswamy
hariharan@iitm.ac.in

[1] Mechanical Engineering, Indian Institute of Technology Madras, Chennai 600036, India

[2] Mechanical Engineering, Indian Institute of Technology Ropar, Punjab 140001, India

and geometry. Ziran et al. demonstrated improved geometric accuracy by employing flat-end tools for select cases of shallow constant wall angle (CWA) components [8]. In ISF, the tool size is constrained by the dimensions of geometric features and the maximum forming loads. Eyckens et al. [9] reported that larger tools exhibit a significantly high forming force at the tooltip. Conversely, smaller tools are more likely to induce material drag due to greater contact friction and surface deterioration. An optimized combination of process parameters (feed rate, tool size, lubrication, sheet material) is recommended for an effective forming in ISF [10–13].

The selection of a toolpath has a crucial role in enhancing the formability of ISF. Several studies have been conducted to explore various toolpath approaches in ISF with the aim of attaining larger draw angles, regulating the material distribution, and mitigating geometrical irregularities [14–17]. The toolpath strategies that have been extensively studied in the past decade include contour (stepped) [18], radial (continuous) [19, 20], feature-based and multi-pass [21, 22] approaches. The commonly used z-slice toolpath follows a series of in-plane passes along the part surface and transitions to the subsequent pass at a constant step depth (d). Although it is convenient, this induces discontinuity in deformation. Filice et al. [3] proposed the use of continuous three-dimensional (3D) toolpaths to avoid the occurrence of such sudden loading discontinuities. The study conducted by Attanasiso et al. [23] focused on examining the optimization of contour toolpath techniques with regard to step depth (δz) and constant scallop height (h). In general, the surface quality improved when reducing δz and h. Barsen et al. [24] evaluated the geometric accuracy of the truncated cone formed by utilizing the KUKA KR21 robotic arm. They preferred helical toolpaths over discontinuous z-level toolpath for superior geometric accuracy. Every toolpath exhibits a unique deformation history, ranging from biaxial deformation at the tool contact to near-plane strain states. This loading history or strain path influences the onset of fracture in incremental forming. The sharp alterations in the tool trajectory also cause material stretching and leave scratch marks. Lee [25] presented an algorithm to generate continuous spiral toolpaths with consistent scallop height. They proposed to eliminate toolpath retractions for an uninterrupted surface milling of free-form surfaces with complex shapes. Harish et al. [26] investigated a fractal geometry-based incremental toolpath (FGBIT) to form a square cup in ISF. Fractal-based space-filling toolpaths show improved formability and more effective material distribution.

Typically, such toolpaths are derived from commercially available computer-aided manufacturing (CAM) software applications like MasterCAM or SolidWorks and imposed directly on the sheet metal in a single-step forming approach with minimum post-processing. Skjoedt et al. [27] generated helical toolpaths using conventional CAM software based on a milling module. The toolpaths developed on CAM software are not optimized to delay fracture or improve geometric accuracy. Malhotra et al. [28] introduced an adaptive slicing algorithm for helical toolpath wherein the step depth is adjusted to minimize the geometric error. This algorithm allowed them to achieve reduced forming time compared to the toolpaths generated using commercial CAM packages for a fixed scallop height.

The aforementioned toolpath approaches primarily relied on layered contours along with the part axis. The influence of tool motion direction on formability for contour toolpaths was investigated by Kopac et al. [29]. They reported that the tool directed inwards from the outer edges of the components tends to improve formability and surface finish. Vanhove et al. [30] investigated the impact of part orientation in relation to the tool axis on the process limits. Lu et al. [31] proposed a feature-based toolpath generation algorithm inspired by the concept of equipotential lines in electrostatics. In this method, toolpath contours are oriented with a tilt proportional to the distance separating the critical edges. Tanaka et al. [32] showed that reorientation of the slicing plane resulted in extended forming limit and improved material distribution.

The part wall angles greatly influence the efficiency of toolpaths in material distribution. Tool pushed across the sheet tends to rapidly thin out the material for larger wall angles compared to lower wall angles. The distribution of thickness in single-step forming is approximated using the sine law [12]. A multi-step forming approach was devised to overcome this constraint imposed by the maximum wall angle. This strategy entails the redistribution of material from the thicker sections to the thinner sections by means of intermediate passes. Hagen et al. [33] employed a multistage forming approach, wherein they generated intermediate shapes by vertically scaling the geometry. Multistage forming was employed to progressively increase the wall angles of the cone to obtain a cylindrical cup. Vanhove et al. [34] and Tanaka et al. [35] validated this approach for cones and pyramids by increasing the wall angles to 90°for AA1050 for single-stage and multistage forming. Li et al. [36] proposed a method to predict the number of multistage passes required by distributing the thinning rate between subsequent passes. Wu et al. [37] analyzed the material motion and the evolution of strain paths in non-axisymmetric components. They improved the geometric accuracy by employing a multi-step toolpath methodology. Zhu et al. [38] attempted to mitigate the occurrence of the fracture and uneven sheet thickness distribution in multistage ISF. They employed a toolpath based on draw angles. Improved dimensional accuracy and thickness distribution were achieved while reducing sinking and bulging significantly. Jung et al. [39] demonstrated the effectiveness of two-stage SPIF in reducing geometric error.

Some efforts have been dedicated to the advancement of toolpath techniques to effectively handle volumetric shape errors and geometric transitions [28]. Verbert et al. [40] proposed feature-based optimized toolpaths to improve the accuracy of the formed parts using the feature detection method for free-form surfaces. Formisano et al. [41] used numerical techniques to optimize the toolpath strategy for polycarbonate sheet deformation to avoid twisting and wrinkling of the part while maintaining a minimum forming force. Gupta et al. [42] utilized a multipass strategy to successfully form a complex part design such as a machine fin. Harish et al. [43] used an adaptive incremental-based toolpath approach for curvilinear geometries. Their approach aimed to improve the thickness distribution by regulating the strains in the critical regions with steeper wall angles.

The process of path planning in incremental forming is complex as it has to ensure that the material does not fail by strain localization. Although there are easily accessible solutions for path planning in industrial activities such as milling, they cannot be directly adopted for ISF applications. The toolpath designer is expected to systematically analyze the CAD model and select the most appropriate sequence for incrementally developing different elements. This process needs to be carried out in a case-by-case manner based on the level of involved complexity. Furthermore, there is a lack of comprehensive research on the correlation between the geometric profile and forming toolpath and their combined impact on the forming process in ISF.

A significant portion of the existing literature on ISF has predominantly relied on independent trial and error approaches while proposing a toolpath. However, the efficacy of such toolpaths for universally applicable shapes remain uncertain. There is a space for extensive research to comprehensively study the selection of an optimal toolpath for components of varying forms and geometries in ISF. Researchers commonly consider convex axis-symmetric shapes within the limits of achievable wall angles for discussing toolpath methods. The development of a suitable tool path becomes crucial when part geometry incorporates asymmetry and local characteristics features.

The outcome of forming, especially the critical forming depth, fracture depth, material distribution (thinning), and geometric deviations, exhibit high sensitivity to the selection of tool path in relation to the specific design of the part. The objective of this study is to systematically examine the efficacy of different tool path options for single-point incremental forming. This study explores the utilization of contour toolpaths with constant z height, spiral tool paths, and less commonly employed toolpath methods such as feature-based and fractal tool paths. The focus is their application in carefully designed part geometries with gradually increasing complexity in the part design with an evaluation of toolpath performance conducted for each individual part.

Methodology

The commonly used tool paths are generated over closed loop slices of a CAD surface model in the horizontal plane with fixed δz (where z is the vertical axis of component) separation. Applicability of such methods faces practical limitations when used for parts with irregular contours, as they cannot capture the local geometrical features effectively. In this context, this investigation is extended to include feature-based toolpaths and space-filling algorithms for comparison. The following subsections describe the key steps involved in developing benchmark shapes and the generation of tool paths using different algorithms.

Designing the shapes for forming

The commonly studied axisymmetrical part geometries, such as a cone or pyramid, are less sensitive to the tool path when compared to non-axisymmetrical part geometry. In order to test and evaluate the performance of the tool paths, four different shapes with distinct geometrical features were utilized, (i) Cone, (ii) variable wall angle conical frustum (VWACF), (iii) asymmetric cone, and (iv) Stepped Conical frustum (Fig. 1).

The geometric changes were progressively included in the typical symmetric part designs (cone, in the present work) to increase the level of asymmetry gradually. All the parts were evolved over a simple (a) cone, (Fig. 1) of 90 mm base diameter and 70° constant wall inclination. Wall angle of 70° (critical angle) is chosen based on iterative experiments to allow maximum forming depth without fracture in cone. Figure 1. (b) i.e., 'VAWCF' is a cone modification with varying wall angle profile ranging from 0° to 90° (with circular generatrix). It is theoretically not possible to successfully develop parts with 90°wall angle features to appreciable depths in a single pass ISF (act as wall angle limit) [22, 44]. VWACF represents a shape with constantly varying wall angle, from 0° at the base to 90° at the top. This design provides an opportunity to evaluate the maximum limit of forming with a constantly changing curvature. Both cone and VWACF are axisymmetric parts. In the third part, Fig. 1(c), an 'asymmetric cone' (henceforth referred as asy-cone) is developed by combining the features of the cone and VWACF along with an inclined top face. Asy-cone has both varying wall angle and constant wall angle sides. The fourth part (Fig. 1d) 'stepped cone' (is designed by introducing a horizontal step feature on the constant wall angle side of asy-cone. This local feature mimics extreme changes in geometric contour, and the capability of toolpath to capture these features can be evaluated. All the parts are designed such that the loading path to fracture is distinctly different from each other. The details of the part dimensions are shown in (Fig. 1).

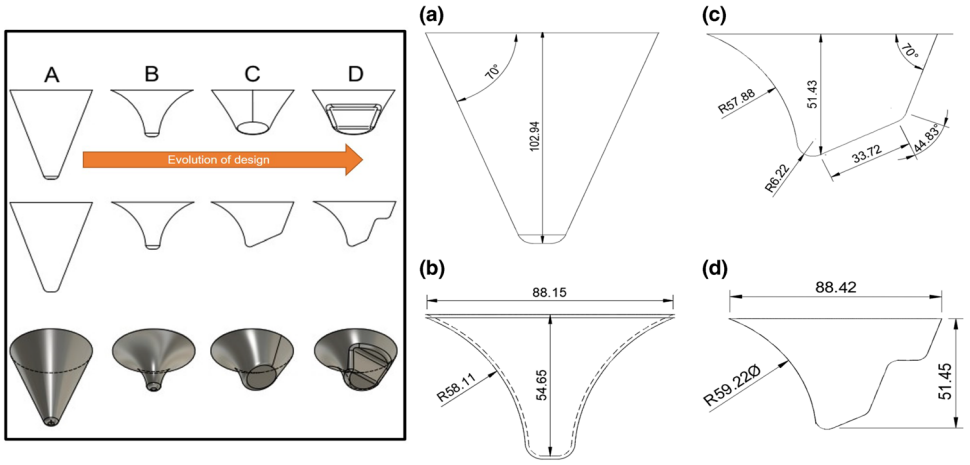

Fig. 1 Part designs for experiments a) Simple cone b) VWACF c) Asymmetrical Cone d) Stepped cone

CAD model segmentation

CAD models in the tessellated formats referred to as stereolithography (STL) formats are used for segmentation and feature extractions for tool path generations (Figs. 2 and 3). Parts are saved in the form of triangular tessellations to define the model surfaces as a group of points. STL format is a widely accepted general-purpose format for CAD data exchange. It is compatible with the commercial software MATLAB™used in the present work to post-process the surface point data. Toolpaths are developed by interpolating lines across surface points along selected contours on the CAD surface for a chosen strategy.

All the strategies mentioned above are discussed in the following subsection.

Toolpath generation algorithm

Stepped toolpath

This work generates a stepped toolpath over sliced contours of the CAD model in the horizontal plane. A fixed distance along the component axis separates these contours. In the rest of the manuscript, the z refers to the axis of the part geometry unless otherwise specified. Toolpath gains incremental depths (δz) only after each complete pass along a contour.

The surface quality of the formed part could be influenced by the separation between consecutive tool passes (contour density). Lower contour density yields coarse tool paths, which could reduce forming time but would give a poor surface finish. For toolpaths based on horizontal slicing, δz values can be calculated for an appropriate scallop height(h) using Eq. 2. A fixed scallop height of $h = 0.05$ mm is maintained to generate contours for all toolpath methods presented here and in subsequent sections.

$$d = \sqrt{r^2 - (r-h)^2} \tag{1}$$

$$\delta z = (2\sqrt{r^2 - (r-h)^2})\cos(\theta) \tag{2}$$

Here, r (5 mm) refers to the tool radius, h (0.05 mm) is the scallop height, $2d$ is the separation between tool sheet contact points along the part wall for two consecutive tool passes, and θ is the inclination of the part wall to the horizontal surface (Fig. 4). Toolpaths developed using the method discussed above are depicted in Fig. 5

The stepped toolpath has the simplest formulation and can be extended to other tool path methods with slight modifications (discussed in the subsequent sections).

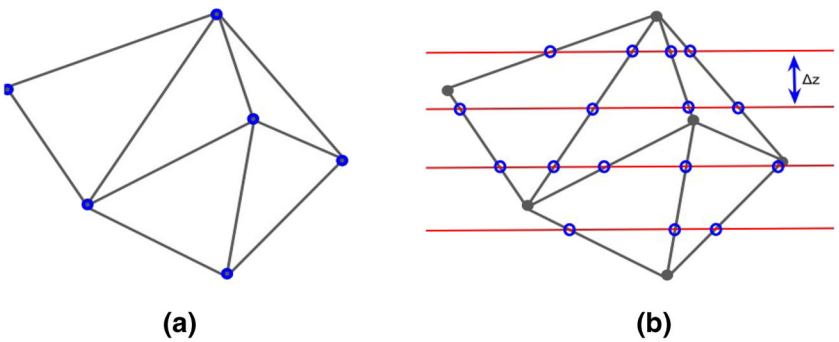

Fig. 2 (a) Segmentation (b) Slicing

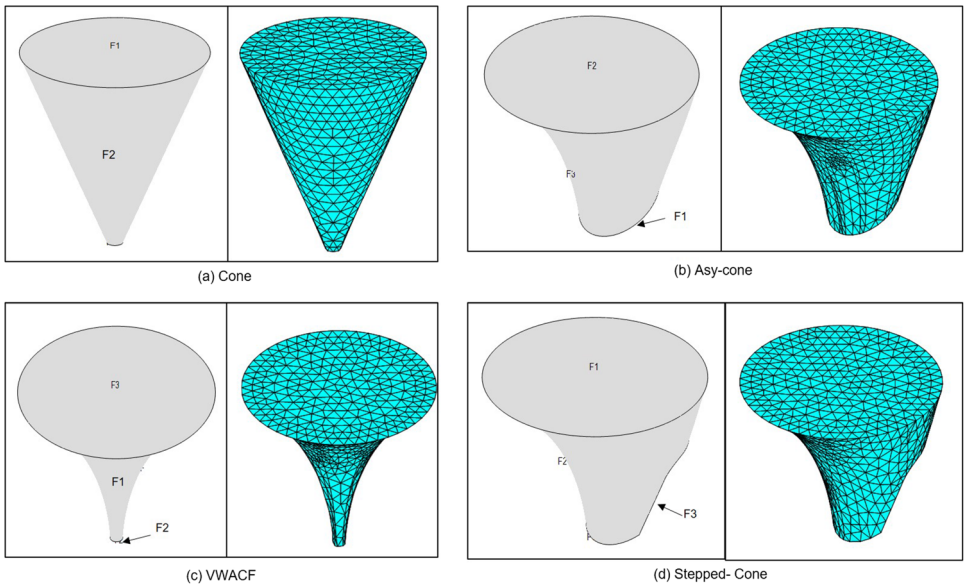

Fig. 3 CAD surfaces (surface 1 (F1), surface 2 (F2) and surface 3 (F3) bound by critical edges) and segmented parts used for ISF

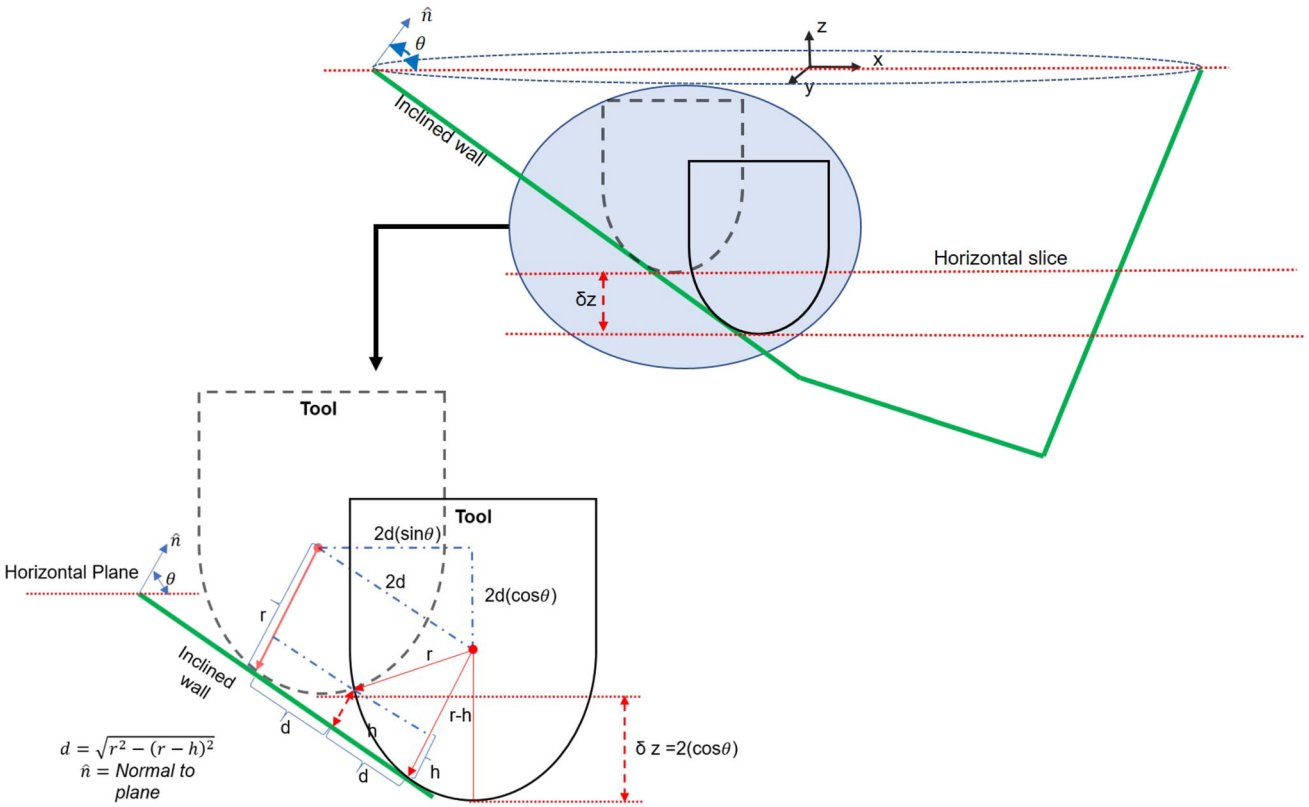

Fig. 4 Schematic of the step toolpath and depiction of the relation between scallop height (h) and step depth (δz) for toolpaths based on horizontal slices

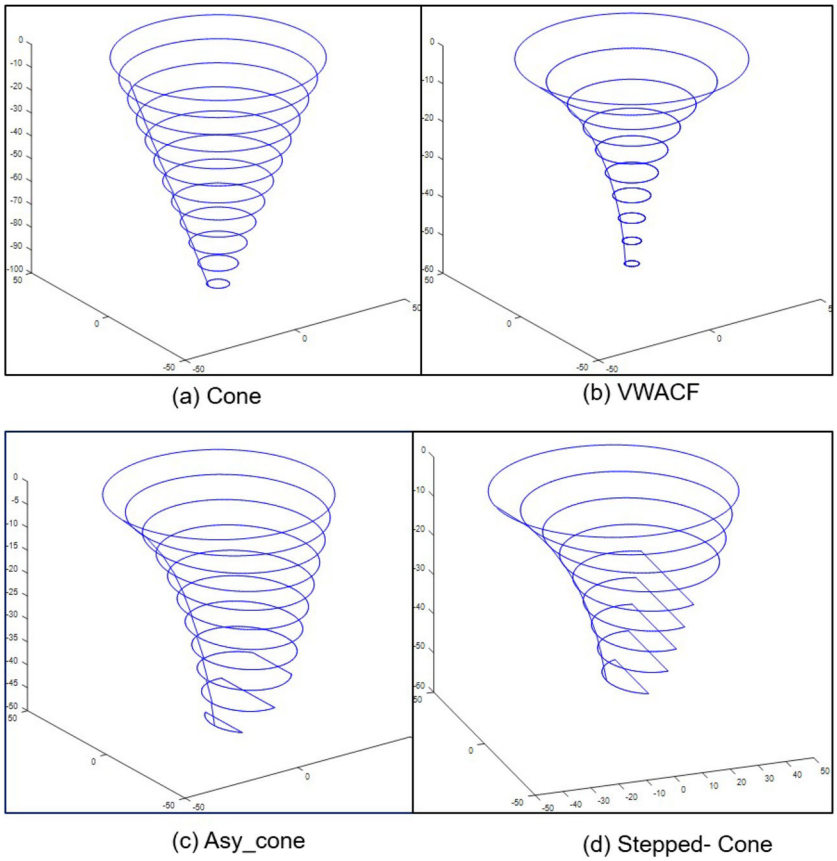

Fig. 5 Depiction of stepped tool(coarse) path developed for the formed components (a) Cone (b) VWACF (c) Asy-cone (d) Stepped-cone (Note: only a few contour lines from the actual toolpath (used for experiments) are shown here for better illustration)

Spiral toolpath

The spiral tool path is continuous with constantly increasing depth along the z axis. As an extension of the stepped toolpath, spirals are interpolations of points between consecutive horizontal contour slices while maintaining a constant scallop height. This interpolation can be linear or of higher order. Figure 6e depicts two slices from the magnified/coarse tool paths to present the interpolations more clearly, which are used to create spirals in this work. The toolpath lines are interpolated between two slices such that the points on each slice are matched with the point closest to them in the subsequent slice. These points on the slices are named as P_{n1}, P_{n2}, ..., P_{ni}, ..., P_{nk}. The first subscript depicts the slice number and the second subscript is the i^{th} point on the n_{th} slice. Therefore, there are 'k' points in the 'n'th slice. Varying weights between (0-1) are assigned such that weight for P_{1i} would be 'w' and weight given to P_{2i} would be $(1 - w)$, where the value by which 'w' increases would be decided by '$\frac{1}{k}$', so the weight 'w' for the i^{th} point would be $((i-1) \cdot \frac{1}{k})$. After assigning weights to each point, coordinates of the intermediate points are determined by adding the weighted coordinates of the points in each set of two slices P_{ni} and $P_{(n+1)i}$, the resultant coordinates make up the interpolated spiral that lie between the 'n^{th}' and the '$(n+1)^{th}$' slice. Figure 6 depicts the spiral toolpaths developed for the formed components.

Feature-based contour tool path

The feature-based algorithm used here is based on an equipotential toolpath concept proposed by Lu et al. [31]. Here, terms like 'voltage', 'equipotential' and 'potential' are used to only describe certain geometrical conditions (and do not carry traditional definitions as stated in the subjects of electrostatics). Contour density definition, voltage assignment to all the points and interpolation of tool-path are the major steps in toolpath generation.

In the feature-based approach, bounding surfaces are identified based on the z-height (along the part depth), which constitute the critical geometrical edges (Edge 1 and Edge 2) for contour generation as illustrated in Fig. 7. All the facets and their vertices are identified from the CAD model. Instead of using a constant z height, a constant distance ratio (d_r) Eq. 3 of tool path contours is associated with each vertex contained within the critical bounding edges.

$$d_r = \frac{d_1}{d_1 - d_2} \tag{3}$$

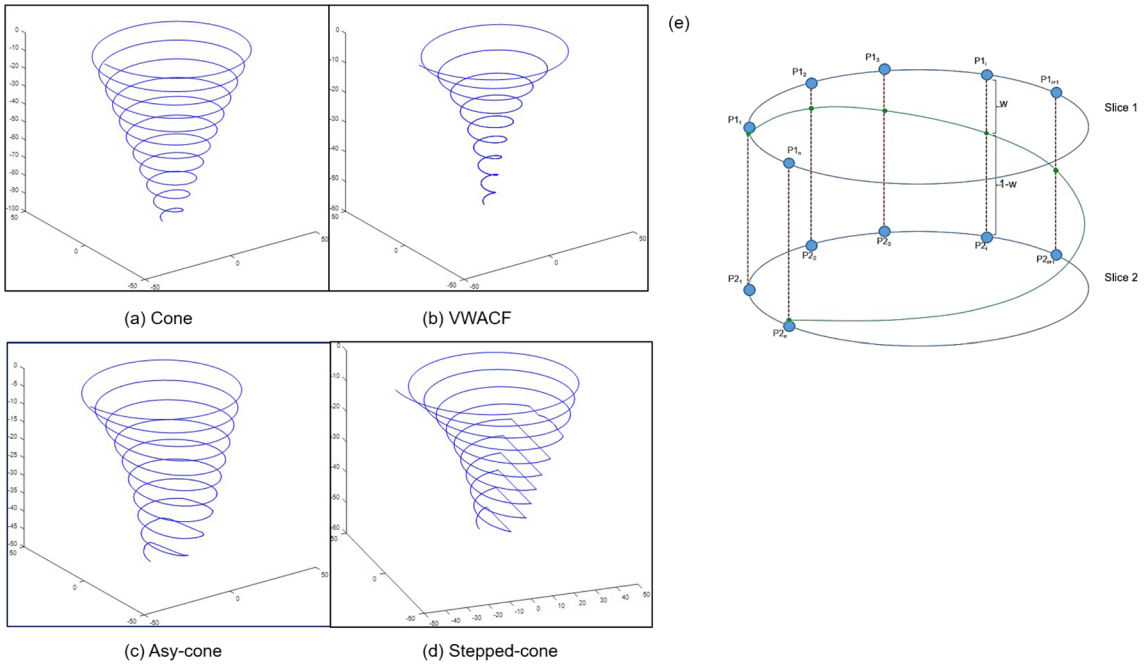

Fig. 6 Depiction of spiral tool (coarse) path developed for the formed components (a) Cone (b) VWACF (c) Asy-cone (d) Stepped-cone (e) interpolation of toolpath across slices for spiral toolpath (Note: only a few contour lines from the actual toolpath (used for experiments) are shown here for better illustration)

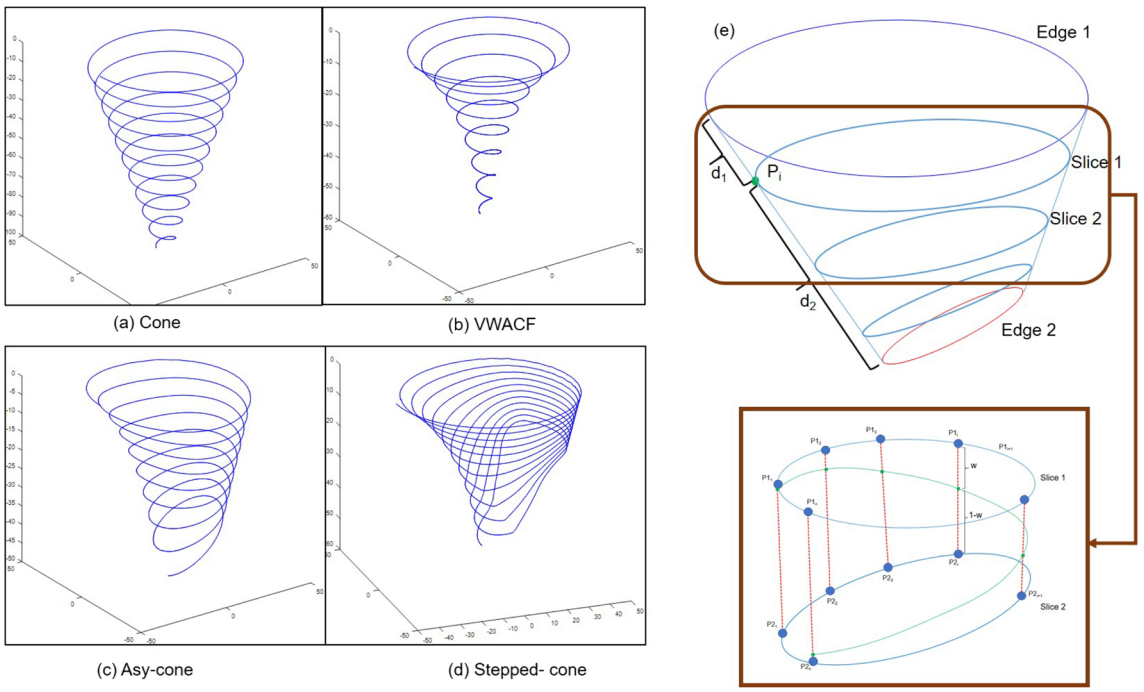

Fig. 7 Depiction of feature-based tool path (coarse) developed for the formed components (a) Cone (b) VWACF (c) Asy-cone (d) Stepped-cone (e) schematic of the toolpath interpolation between non-horizontal slices (Note: only a few contour lines from the actual toolpath (used for experiments) are shown here for better illustration)

Here, d_1 and d_2 are the distance of any point on the surface of the CAD model from Edge 1 and Edge 2 respectively. From Eq. 3, the value of d_r lies between 0 and 1. Points with the same d_r values are assembled.

Then, a linear spiral interpolation is applied between each consecutive slicing plane, similar to what was done in Section 2.3.3, to get the equipotential path. The contour slices in the stepped and spiral toolpath are horizontal and independent of the part's geometric features. In the case of the feature-based toolpath method used here, the slices assume an arbitrary orientation to accommodate changes in the feature of the part geometry (Fig. 7e). The contour slices tend to orient more towards the edges with increasing depth, as depicted for illustration in (Fig. 7e). The feature-based algorithm is more sensitive to the part asymmetry and can prove to be more efficient with uniform material distribution. Figure 7a-d depicts toolpaths generated using the above strategy for parts formed by ISF. This toolpath method is expected to be theoretically the same as a spiral toolpath for axis-symmetric profiles; however, the difference between them is truly illustrated in the case of asymmetric parts.

Fractal toolpath

Fractal tool paths are introduced with the idea of space-filling toolpaths built over contour slices, mainly to engage a larger material for the same volume of part deformed. Compared to stepped or spiral toolpaths, the material is deformed multiple times in a space-filling strategy until the forming is completed.

The CAD model is sliced into multiple layers along the vertical axis (z-axis) while maintaining a constant scallop height (0.05 mm) condition (similar to the Step toolpath strategy), and then the area enclosed by each slice is filled with the Hilbert curve (Fig. 8). Hilbert curves allow isotropic material distribution and are easy to implement in CNC, making them a good choice for ISF applications. Hilbert curves fill a square area with repeating patterns which increase by a factor of four for each increment in the order of the fractal (Fig. 9a).

The order of the fractal is controls the density of the toolpath, which is, in turn, dependent on the scallop height decided by the user. The role of scallop height in deciding fractal density is illustrated in (Fig. 9b) Eq. 4.

$$2^n = \frac{D}{2\sqrt{2rh - h^2}} \tag{4}$$

Here, n is the order of the fractal, D is the maximum dimension in the part design, r is the radius of the tool and h is the scallop height. The space-filling curves are stitched to contour boundaries for irregular shape contours to avoid path discontinuities and allow a smooth surface quality. This is illustrated in Fig. 10 for a cross-section with a concave feature. The stitched path over each contour is stacked layer by layer to obtain a three-dimensional path. Figure 11 depicts the toolpaths generated by the fractal algorithm discussed above for the formed components. The coordinates of the connected points are converted to a GCode to be read by the CNC machine.

Compensation

Generally, the toolpath is generated for the initial point of contact between the tool-tip and the sheet metal. However, for a fixed axis tool orientation, the contact point shifts along the tool surface based on the changes in the part feature. Such a change in contact point coordinate is incorporated into all the toolpath methods by estimating the appropriate compensation.

For a spherical tool, the sheet is assumed to always maintain tangency at the point of contact with the direction normal of the CAD Model, co-linear with the tool center. As illustrated by Fig. 12, the direction cosines of the surface normal vector provide the angular reference (α, β, γ) to compensate

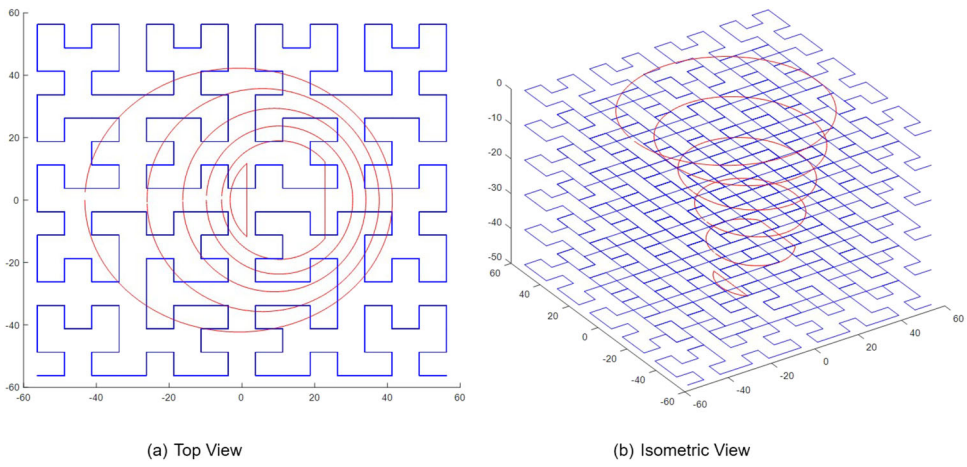

Fig. 8 (a) Fractal toolpath top view (b) Layered slices of fractal toolpath depicted for Asy-cone part

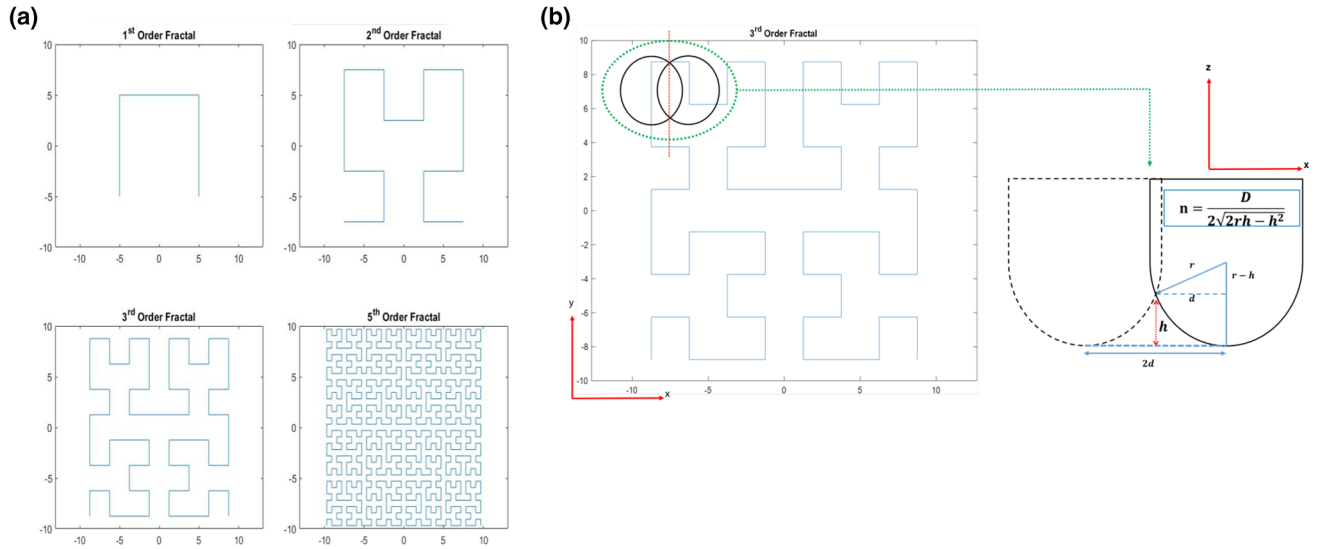

Fig. 9 (a)Illustrates the order of fractals (b) depicts the calculation of fractal density

the tool point of contact. Similar compensation strategies can be applied to non-spherical tools as well.

Experiments on single point incremental forming

Single point incremental forming (SPIF) experiments were performed in a 'Jyoti Huron KMill' CNC machining center using AA1050 blanks of dimension 150 mm×150mm×1.2 mm. The mechanical behavior was characterized by a uniaxial tension test using a 100 kN capacity (Zwick-Roell 100) universal testing machine (UTM) at $0.005s^{-1}$ strain rate (Fig. 13). Mechanical properties of AA1050 are presented in the Table 1.

A customized fixture rigidly held the sheet metal blank with a blank holding plate (work area of 100 mm × 100 mm) to avoid material draw-in during forming. A simple forming tool (non-rotating) with a 10 mm diameter hemispherical ball end was forced across the sheet surface along a programmed path at a constant feed rate of 750 mm/min. All tool trajectories were computed by coding the toolpath algorithms in MATLAB. Contact friction was kept at a minimum by applying a layer of hydraulic oil at the tool sheet interface. The experimental setup is shown in Fig. 14.

Fixed scallop height and constant δz were maintained across the tool path strategies. The details of the toolpath generation algorithms are discussed in the Section 2.3. All deformed parts were digitized by (HEXAGON|8325-7 with RS5) laser scanner and compared with nominal CAD models for estimation of wall thinning and geometrical deviations using PolyWorks|Inspector™metrology suit. (Discussed in the section following sections)

Results and discussion

An ideal tool path design should aim to simultaneously improve the geometric accuracy of the part shape and the formability of the component. The performance of the tool path strategies (Section 2.3) is evaluated by comparing experimental output with the original CAD model of the part. The mode of failure in incremental forming is a combination of local necking and ductile fracture [45]. Therefore, the dis-

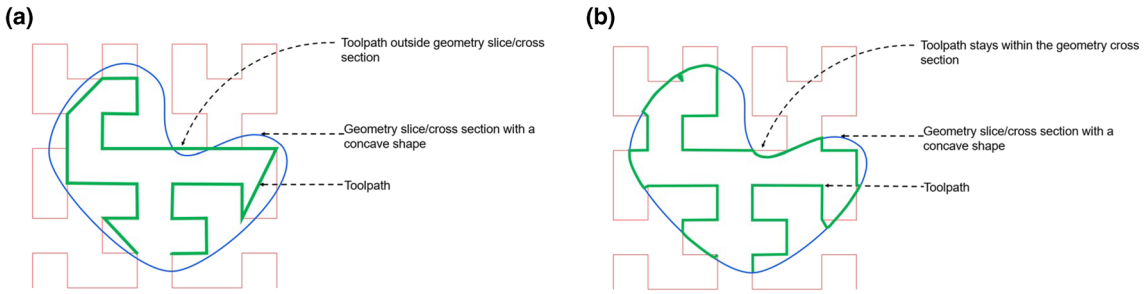

Fig. 10 (a) Without intermittent path stitching (b) with intermittent path stitching

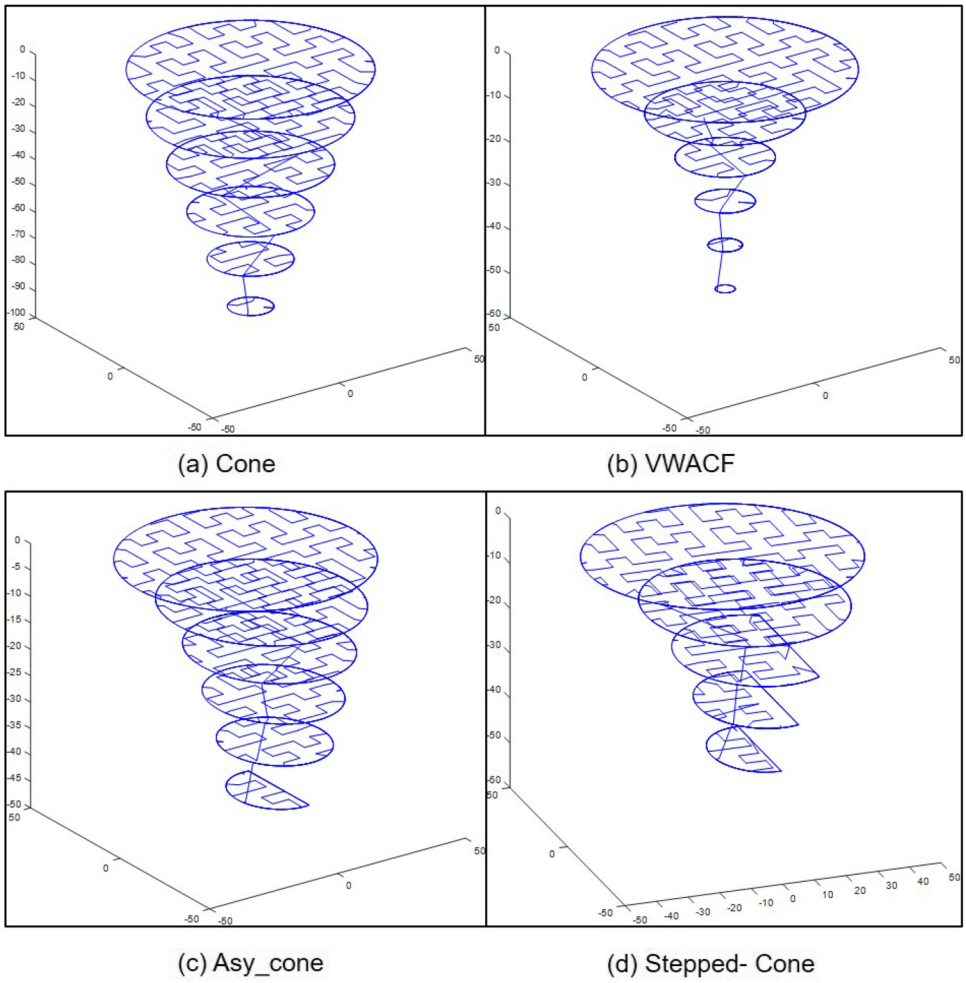

Fig. 11 Depiction of fractal tool path (coarse) developed for the formed components (a) Cone (b) VWACF (c) Asy-cone (d) Stepped-cone (Note: only a few contour slices from the actual toolpath (used for experiments) are shown here for better illustration)

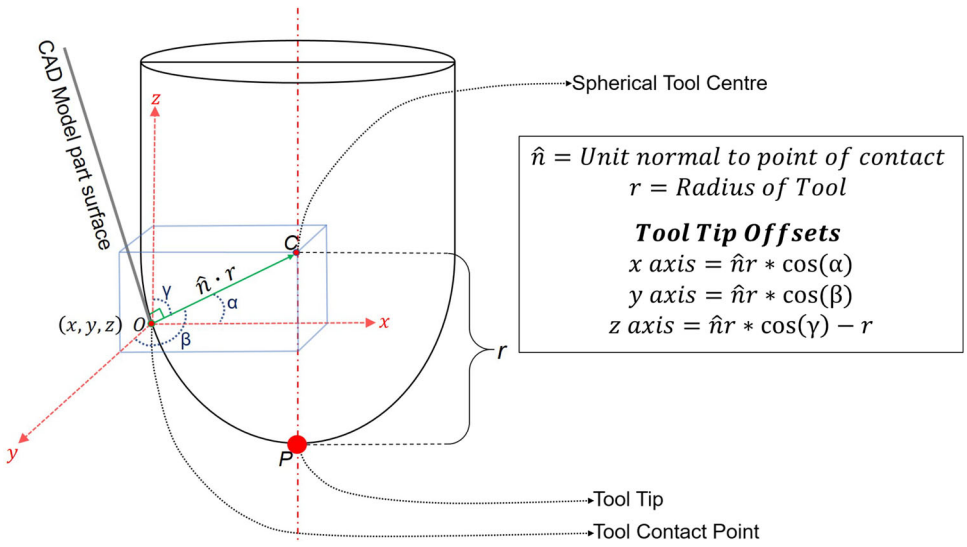

Fig. 12 Tool-tip offset calculation

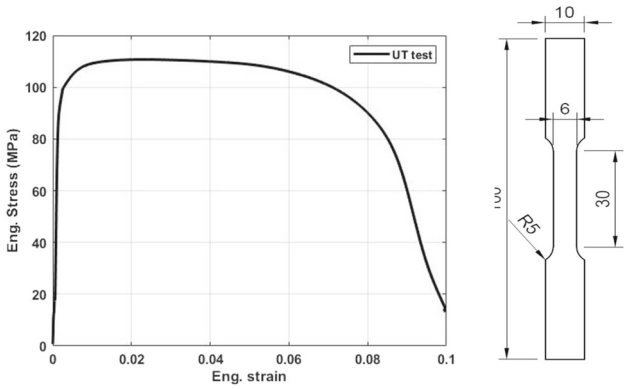

Fig. 13 Stress-Strain behaviour of AA1050 from uniaxial tension test

tribution of thickness and depth of fracture is compared for different tool path algorithms. Uniform thickness and higher depth of fracture indicate better formability. The results are discussed individually for each attribute and compared in the following sections. At least three measurements are taken for each location. The average error due to possible scattering during data collection is calculated by dividing the standard deviation by the square root of a number of measurements.

Thickness distribution

The material distribution during deformation is expected to vary with the tool path. This can be quantified by thickness reduction. The measure of thickness reduction also facilitates the assessment of failure mode. The deformed parts are digitized by laser scanning, and the scanned models are compared with the nominal CAD profiles (Figs. 15, 16, 17, 18, 19, 20, 21, and 22). For a thorough understanding of the material distribution, thickness variation is checked circumferentially (along the horizontal plane at each z- level) and axially (along the part depth) for the formed components. Color contours (Figs. 15, 17, 19 and 21 provide a very good depiction of the circumferential thickness distribution at each z-height level.

As all the continuous toolpaths are predominantly guided by the final CAD profile, the asymmetry in the part is bound to be reflected in the pattern of material distribution in the formed component. It can be easily verified, as in the case of cone and VWACF; the axis-symmetricity of the design allowed uniform circumferential material distribution at every depth for all four toolpaths. A similar investigation, when extended to parts with increased asymmetry (Asy-cone and Step-cone), showed significant variation in circumstantial thickness. It can be inferred that irrespective of the toolpath strategy (horizontal slicing-based (spiral, step, fractal) and feature-based algorithms), circumferential thickness variation is minimum for axis-symmetric parts.

Table 1 Mechanical properties of aluminum AA1050

E (GPa)	YS (MPa)	UTS (MPa)	Poisson's ratio	Elongation(%)	
				uniform	fracture
71.659	101.914	113.2987	0.33	2.31	9.96

Furthermore, local changes in geometrical features (here, wall angle) also have a very prominent effect on the achieved final thickness and the rate of material thinning. As depicted in (Fig. 16a), for constant wall angle profiles, a narrow region closer to the base of the cone (at z = 0) registers the maximum rate of thickness reduction. Such a change can be attributed to a sharp change in the wall angle from 0° to 70°, which develops a region of increased strain. Localized thinning is marked by the sudden drop in the thickness values (Figs. 16, 20e). The wall thickness tends to stabilize to a constant average value ranging from 0.44 mm to 0.51 mm for all toolpaths during the subsequent deformation of the cone profile (with a constant wall angle 70°).

It can be observed that the 'stepped toolpath'(z-slice) allows maximum overall deformed wall thickness and the spiral toolpaths the minimum with a difference of 0.1 mm for constant wall angle profiles.

As mentioned earlier, the wall angle varies gradually between 0° to 90° in variable wall angle conical frustum (VWACF). In this case, a gradual thinning is seen for all toolpaths without notable local thinning, unlike for constant wall angle profiles (Cone)(Fig. 16e). This observation is crucial in understanding the role of changes in geometric features in regulating the rate of material thinning. A similar thinning trend is observed for the Asy-cone (with both CWA and VWA) profiles, where a region of local thinning appears at the CWA side, contrary to VWA profile, where the wall thickness reduced more gradually, as can be seen in Fig. 20(a,b). Such thinning behavior is expected to be feature-dominated as the experiments yield similar thickness trends for all the toolpath strategies.

Figure 21(a,b) is the contour plot depicting the thickness distribution for the 'stepped-cone'. The part has a local horizontal step on the constant wall angle side. This horizontal step further increases the part complexity by introducing irregular feature evolution. Such sudden changes bring out the most thickness variation in the feature-based toolpaths. Also, the region of local thinning is reduced on the CWA side for feature-based toolpath (Fig. 22a) and tends to shift towards the VWA profile. Such a change can be attributed to the toolpath generation algorithm. As the feature-based toolpath lines are generated over non-horizontal slice planes (unlike step, spiral, and fractal toolpaths), which are oriented based on the distance between the critical edges (Section 2.3.3). The contour lines tend to trace deeper profiles in the features with larger depths. This leads to greater wall thinning in the deeper contours because of a larger variation of

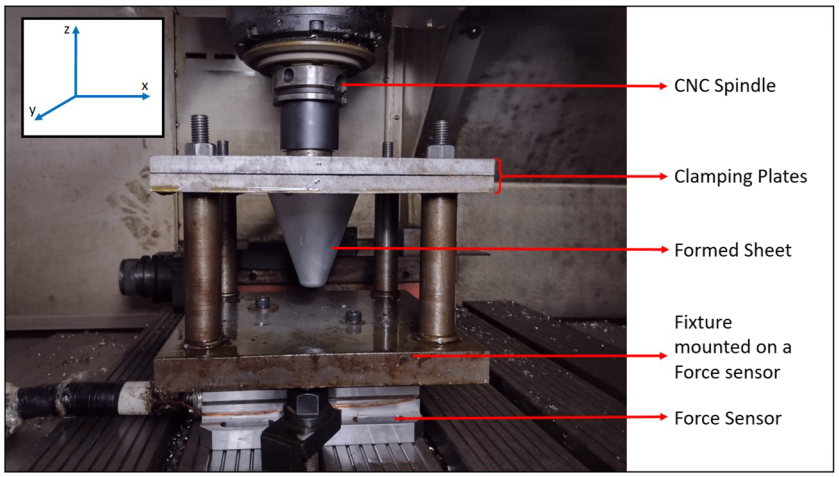

Fig. 14 Experimental setup used for ISF

δz increments per pass of the tool. Such patterns are not observed for toolpaths based on horizontal contours.

An overall observation of material distribution across all part profiles, suggests that spiral and feature-based toolpaths allow a more uniform thickness along the horizontal cross-section (circumferential). Whereas z-slicing and fractal toolpaths have a slightly uneven thickness distribution, due to the sharp changes in tool direction while deformation. Fractal toolpaths allow more material flow around the curved geometries along the depth compared to other methods. However, its performance around the CWA profiles is similar to other toolpaths.

Geometric deviation

The formed parts are scanned using a laser displacement sensor to examine the geometric accuracy. The point cloud is imported as a .stl format polygonal model and compared with the nominal CAD model. The evolution of geometric deviations measured along the part depth are depicted in Figs. 23, 24, 25, 26e,f, along with deviation contour plots (Figs. 23, 24, 25, 26a-d) for all formed components.

Both geometrical features and toolpath methods individually influence the geometric deviations. Significant part deviations are seen at the initial deformation stage at the

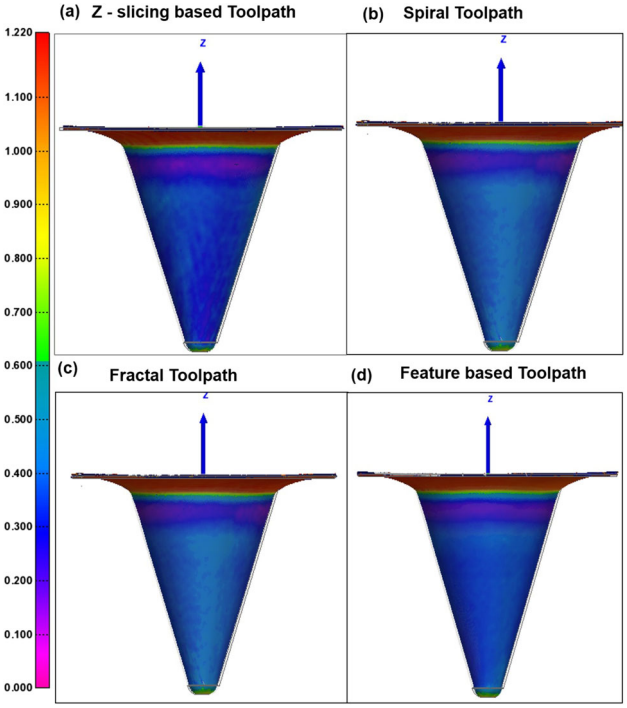

Fig. 15 (a-d) Color contour plots for thickness distribution for Cone

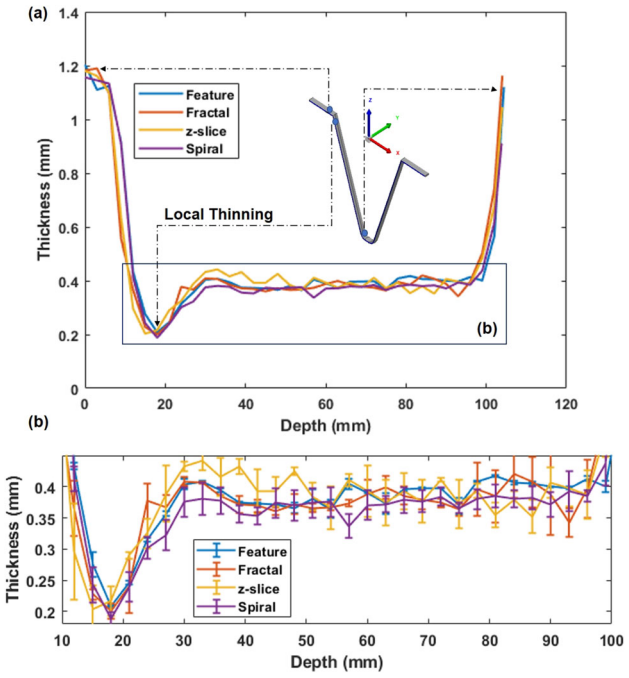

Fig. 16 (a) Thickness variation along the vertical (z-axis) cross-section (b) plot of the selected section with the error bars

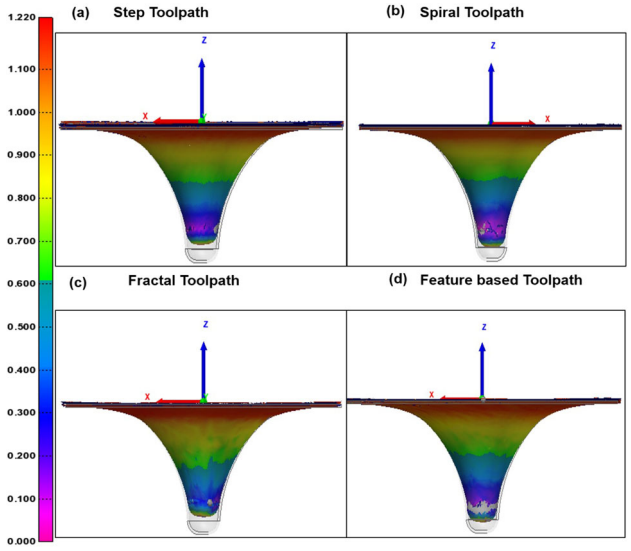

Fig. 17 (a-d) Color contour plots for thickness distribution for VWACF

part base (z=0). This is largely due to the local bending of the unsupported sheet around the tool. Such deviations are marked positive in the color scale as it leaves the final part dimensions larger than the nominal and are caused mainly due to bending of the sheet.

The amount of geometric deviation in the formed component can be directly attributed to a particular toolpath strategy by the way of imposed strain. Each toolpath method leaves a unique strain history for the duration of forming, which is reflected in the evolution of thickness stains. The recoverable strains in the deformation process contribute to the deviations due to material springback. Also, the thinning percentage scales with local strains caused during incremental forming. It is very evident from the Figs. 23, 24, 25, 26e,f, that a larger variation in thickness distribution is reflected in in-homogeneous thickness strain distribution. This can be related to increased springback.

A closer observation can reveal that negative geometric deviations are common to the CWA profiles near the region of local thinning. This is mainly influenced by the increased local stains due to the drastic change in the feature (from 0° to 70° in a cone). Whereas, for gradually changing profiles (VWACF), such deviations are not observed, and are mainly due to the local bending of the sheet.

All toolpaths performance is comparable within (0.4 mm to -0.6 mm) with very minute differences in geometric deviations only significant to the second decimal place. It is also observed that the z-slice(step toolpaths) allows the least geometric deviations for regions/parts with CWAs. On the other hand, feature-based toolpaths are able to achieve more uniform strain evolution with better geometrical control for VWA profiles for axis-symmetric components. However, with increased asymmetry in the part design fractal-based toolpath method appears to achieve better dimensional control with lesser overall deviations. Also, in space-filling toolpaths methods (fractal) larger material is engaged by the tool and repeated deformation increases the effect of strain hardening. These factors are expected to reduce the overall material spring back. However, an increase in deviation is observed around areas with maximum thinning. The performance of toolpaths in capturing the step feature in the 'step-cone' is also evaluated. An issue of sheet bending is also observed at the transition from flat to angle in the wall profile for all the horizontal slicing-based toolpath methods. However, the flat region is underdeveloped for feature-based toolpath until part failures.

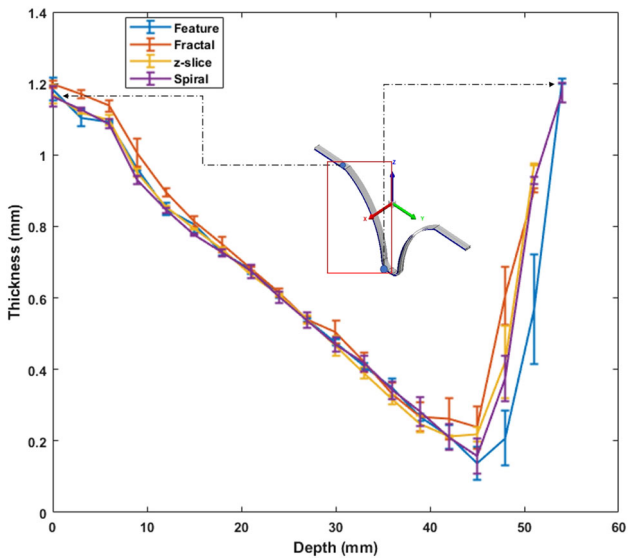

Fig. 18 Thickness variation along the vertical (z-axis) cross-section

Formed depth

Toolpaths are also evaluated for formability, by their effect on the forming depth (marked by the occurrence of fracture) for all part shapes. Gradual thinning of the part during ISF leads to eventual fracture, which is the limit for the achievable depth for the chosen forming parameters. Figure 27 depicts the forming depths achieved for all the shapes developed using each toolpath method.

Cone and VWACF are widely chosen geometry for the validation of the incremental forming process, and in this work, they are designed to form until their maximum limits.

Cones are successfully formed to the designed depth without any visible fracture; however, a slight difference is recorded in the part depth across all toolpaths (Fig. 27a). A maximum depth of 101.706 mm is obtained for the fractal toolpath. The absence of failure and larger formed depth in the cone can indicate that space-filling (fractal-based) tool-

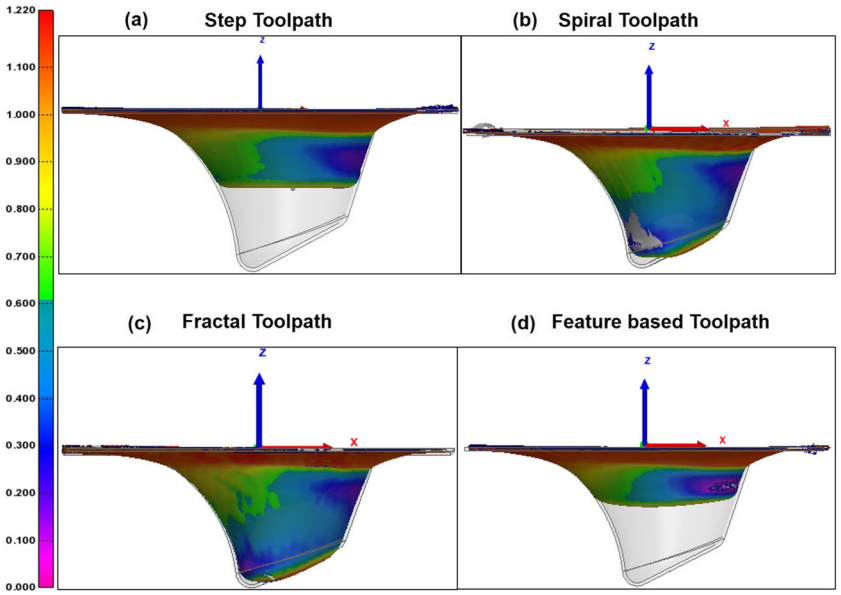

Fig. 19 (a-d) Color contour plots for thickness distribution for Asy-cone

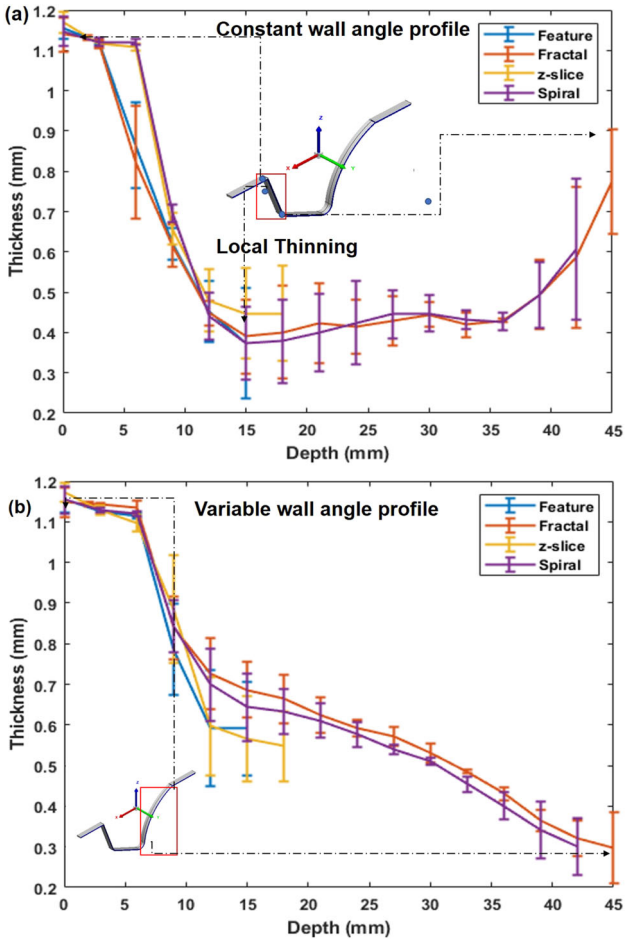

Fig. 20 Thickness variation along the vertical (z-axis) cross-section for (a) CWA (b) VWA profiles

paths are able to maintain minimum spring back for CWA profiles.

In the case of VWACF, the wall thickness decreases gradually until fracture at critical wall angles as depicted in (Fig. 18). With an overall difference of 0.7 mm, minimum fracture depth is obtained for the fractal toolpaths (42.083 mm), while for feature-based and spiral toolpaths, fracture depths are very close with 43.613 mm and 43.807 mm, respectively (Fig. 27b). Although we see minute differences in fracture depths, they are minimal for axis-symmetric components for all toolpaths studied here. This is theoretically expected because, for axis-symmetric components (Cone and VWACF), all toolpath algorithms tend to generate parallel contours while maintaining a constant scallop height condition, resulting in a uniform contour density (Figs. 6, 9).

The inclusion of slight asymmetry in part (Ays-Cone) allowed us to observe the influence of geometric asymmetry on formed depth distinctly. An early fracture was observed for the z -slicing (18 mm) and feature-based method (15 mm) (Fig. 27c). Due to the asymmetry of the part, non-uniform thinning is observed around the features with constant wall angles for feature-based toolpaths. However, spiral and fractal toolpaths allowed maximum deformation with fracture depths up to 39 mm and 33 mm, respectively. Feature-based toolpath performs the poorest in terms of overall fracture depth for asy-cone.

It is apparent that adding a flat feature in the step-cone allows a small relief from continuous local thinning and prevents earlier failure as otherwise seen in the case of asy-cone (Fig. 27c and d). However, parts with larger asymmetry suffer from irregular thinning by feature-based toolpath, and localized thinning along the deeper features cause failure (32.443 mm) before the critical limits. Step (z-slicing) and spiral tool-

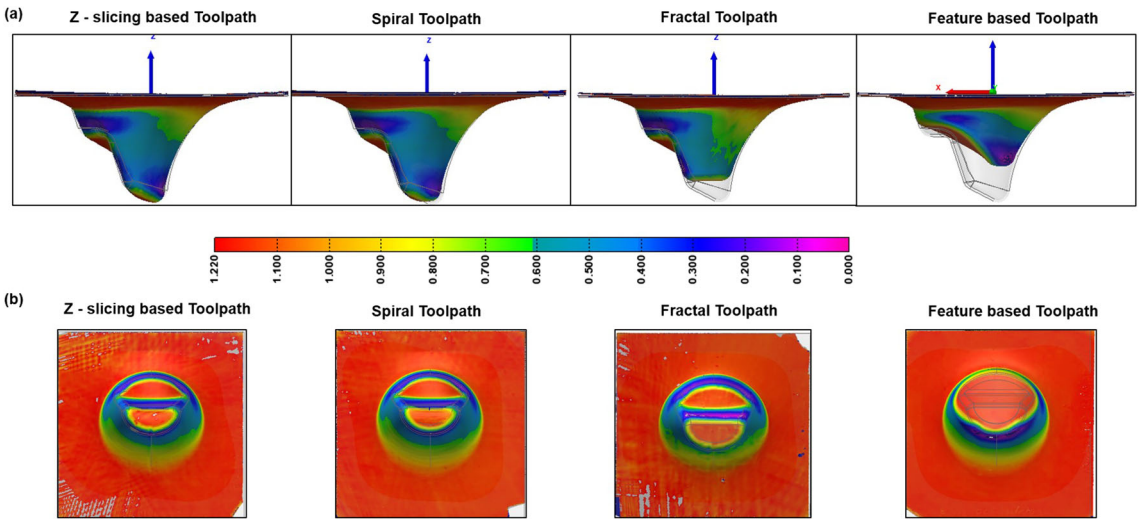

Fig. 21 (a) Thickness distribution for stepped Cone (b) thickness distribution top view

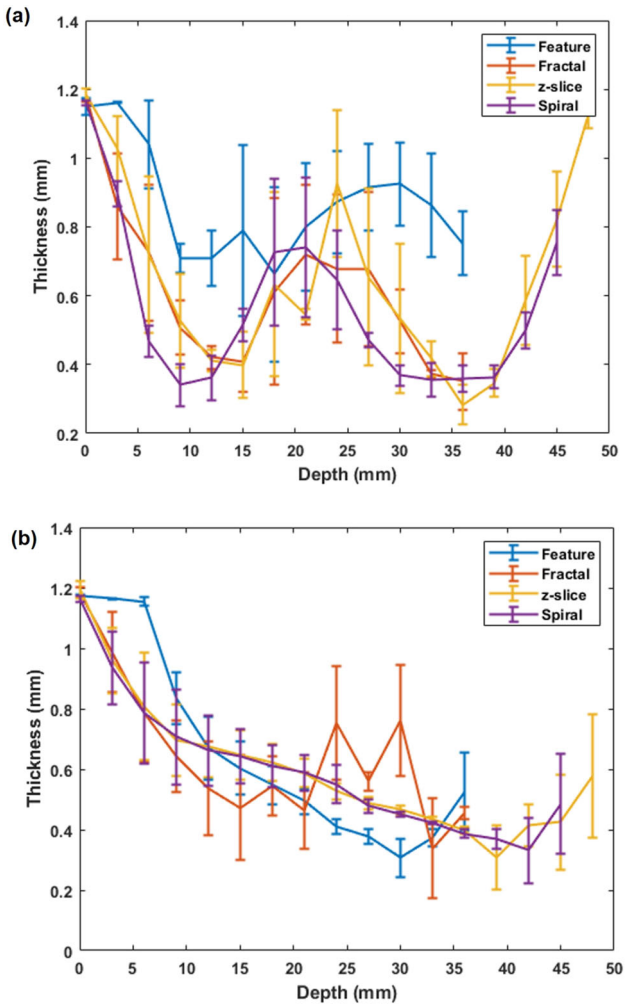

Fig. 22 Thickness distribution for stepped Cone (a) along CWA and (b) along VWA profiles

paths successfully delay the fracture until it is closer to the designed depth, with a fracture at the bottom end at 40.07 mm and 41.474 mm, respectively. The spiral toolpath gives the maximum depth.

Comparative assessment

The systematic assessment of the geometric deviation, thickness distribution, and the formed depth for each component provides insight into the relative performance of the toolpath. For a comparative judgment, the overall mean thickness distribution and geometric deviation for each profile case are presented in the table below Table 2.

All parts depict various profile combinations possible within typical sheet metal components based on a conical base. The cone and VWACF represent part cases with constant wall angle profiles, respectively. Asy-cone has portions of both constant wall angles and VWA profiles, and the Step cone is an extension of asy-cone with a flat feature. The observations of this study can be extended to provide useful insight into the possible selections for the toolpath methods suitable for the goal of maximum thickness distribution and formed depth and minimum geometric deviation for various profile cases Table 3.

It can be recommended that for a more complex part shape, a combination of toolpaths can be used to achieve specific objectives of minimum geometric deviations and maximum fracture depth. For most cases, the spiral toolpath tends to give the highest formability with maximum formed depth.

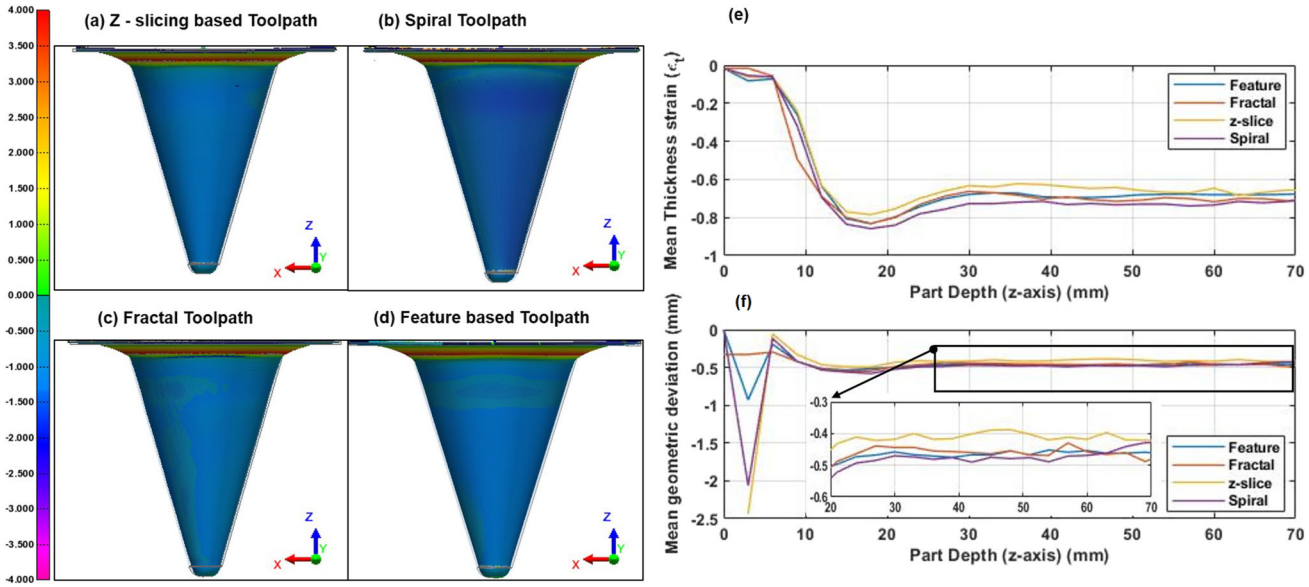

Fig. 23 (a-d) Geometric Deviation contour plots (e) thickness strain distribution and (f) Geometric deviations plots along the part depth (z-axis) for cone for all toolpaths

Conclusion

In this work, a systematic investigation has been undertaken to evaluate the performance of different tool path strategies on SPIF. This work compares conventional z- slice and spiral toolpaths with one of the feature-based tool path strategies and space-filling fractal tool paths to develop complex asymmetric sheet metal components. The influence of different strategies was studied to understand the forming behavior. All toolpath strategies were evaluated using four components designed with gradually increasing asymmetry for material distribution, geometric accuracy, and fracture

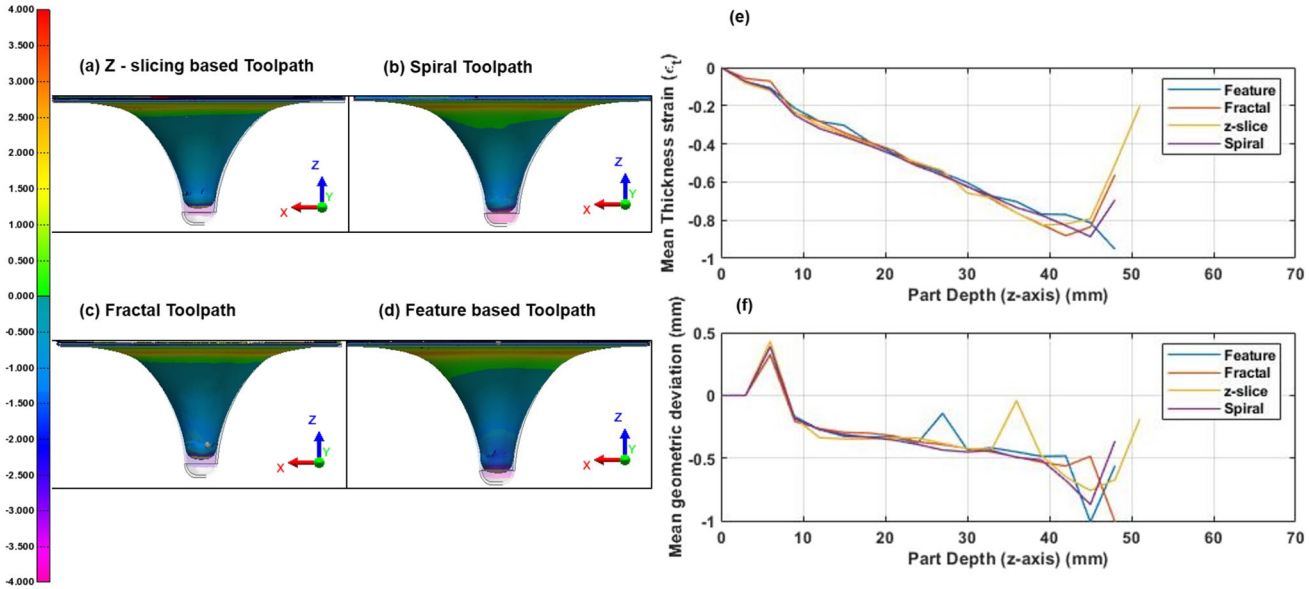

Fig. 24 (a-d) Geometric Deviation contour plots (e) thickness strain distribution and (f) Geometric deviations plots along the part depth (z-axis) for VWACF for all toolpaths

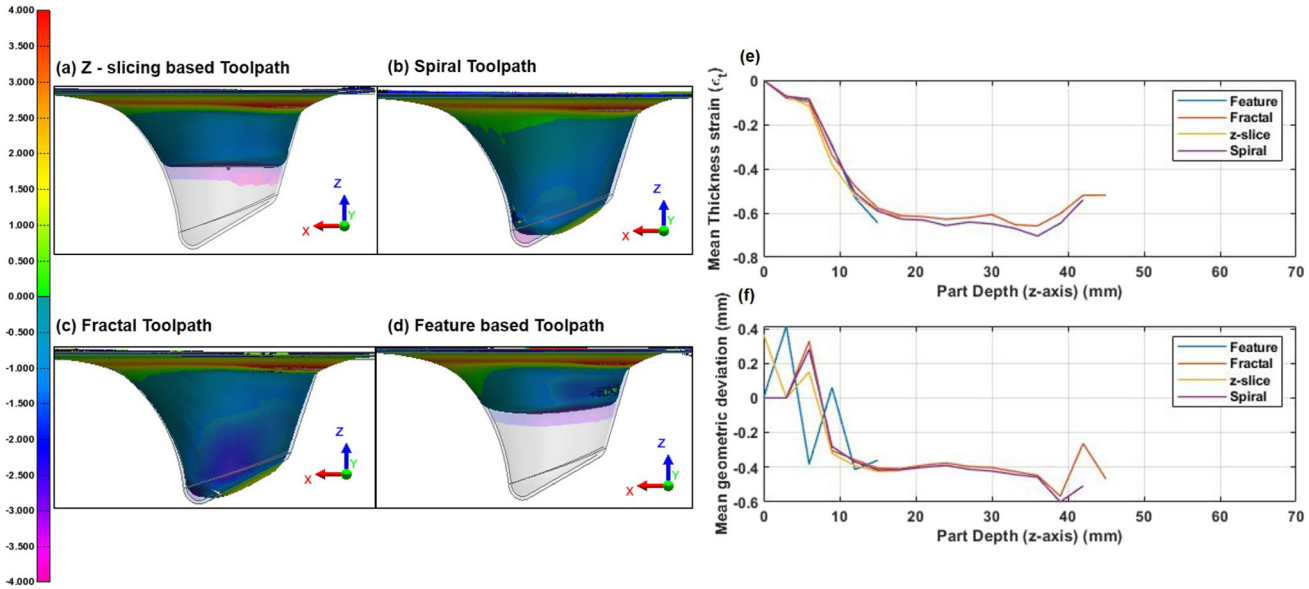

Fig. 25 (a-d) Geometric Deviation contour plots (e) thickness strain distribution and (f) Geometric deviations plots along the part depth (z-axis) for Asy-cone for all toolpaths

depth. The outcome of forming, especially the parameters like critical forming depth, fracture depth, material distribution (thinning), and geometric deviations, are highly sensitive to the choice of tool path for a given part design. The results suggest that the material is stretched differently for different toolpath strategies, which is evident from the overall material distribution and geometric deviations. Fractal toolpaths exhibit a high computational demand, and the forming time is significantly higher compared to other toolpaths for the same component. The primary objective of the present work is to investigate the influence of toolpaths on the deformation mechanics within a specific experimental setting. Therefore exploration and optimization of parameters such as lubrication for certain toolpath have not been undertaken. It is shown that for asymmetric shapes, the fractal path caused premature failure. But the thinning distribution is not as uniformly spread as the spiral path. This indicates the possibility of further enhancing the formability by modifying the lubrica-

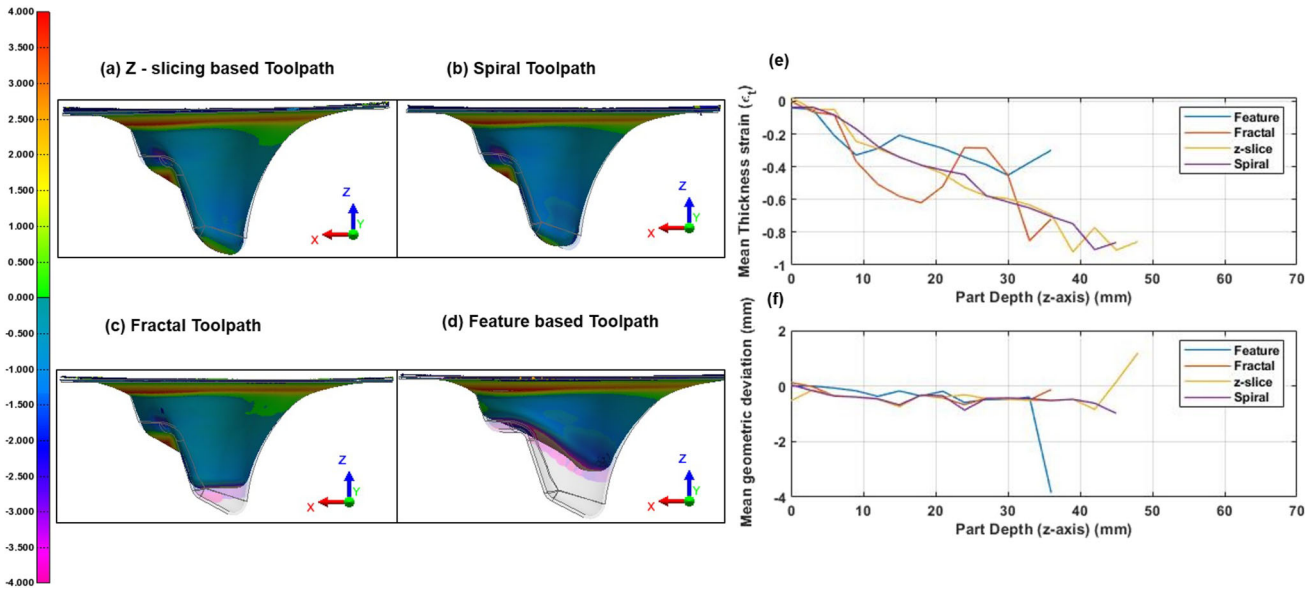

Fig. 26 (a-d) Geometric Deviation contour plots (e) thickness strain distribution and (f) Geometric deviations plots along the part depth (z-axis) for step-cone for all toolpaths

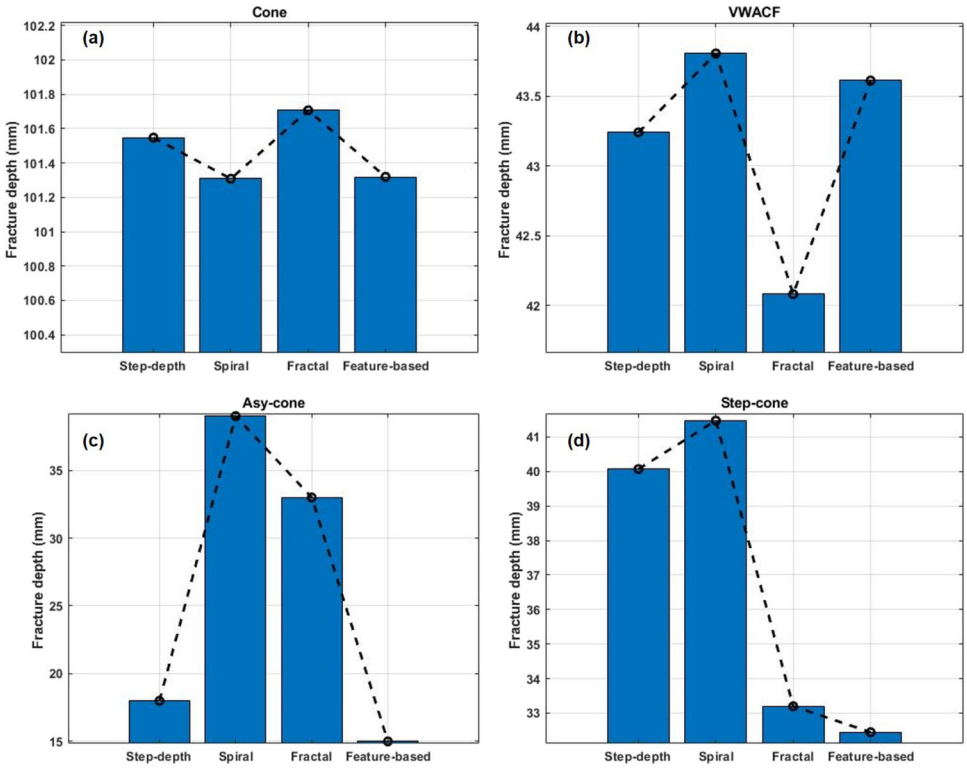

Fig. 27 Experimental fracture depth achieved for the formed components (a) Cone (b) VWACF (c) Asy-Cone (d) Stepped- Cone

Table 2 Mean Thickness and geometric deviation and formed depth for each toolpath method presented for the formed components

Cone Toolpath	Mean Thickness (mm)	Mean Deviation (mm)	Formed depth (mm)
Feature	0.480	-0.461	103.9
Fractal	0.460	-0.467	104.2
Step	0.507	-0.405	104
Spiral	0.442	-0.448	104
VWACF			
Feature	0.646	-0.254	43.4
Fractal	0.656	-0.284	42
Step	0.661	-0.256	43.5
Spiral	0.671	-0.270	43
Asym. Cone			
Feature	0.888	-0.239	15.4
Fractal	0.900	-0.369	42.6
Step	0.877	-0.445	18
Spiral	0.904	-0.341	44.7
Step Cone			
Feature	0.890	-0.708	32
Fractal	0.719	-0.451	37.2
Step	0.626	-0.462	46.3
Spiral	0.666	-0.493	47.2

tion. Such efforts to maximize formability by combining tool path strategy and process parameters will be investigated in the future. Some interesting observations based on the case study are listed below:

1. The local changes in part features (wall angles) has a very prominent effect on the achieved final thickness and the rate of material thinning at the tool contact point. The thinning rate is directly proportional to the degree of change in part features. With the rapid change in wall angle from 0° to 70° in the cone, the thickness drops to 0.2 mm locally compared to 0.6 mm for VWACF with gradually changing wall angles.
2. The feature-based tool path strategies are expected to capture the part curvatures more uniformly, leading to

Table 3 Selection table for toolpath method for various profile case combinations (1) Constant wall angle (CWA) (2) Varying wall angle (VWA) (3) CWA + VWA (4) CWA +VWA + Flat feature

Parameter	CWA	VWA	CWA + VWA	CWA +VWA + Flat feature
Max mean thickness	Step	Spiral	Spiral	Feature
Min. mean geo.Dev	Step	Feature	Feature	Fractal
Max formed depth	Fractal	Step	Spiral	Spiral

uniform material thinning for curved features. However, with the increase in asymmetry, feature-based toolpath tends to induce localized thinning in the deeper regions of the part. Spiral and step-depth toolpaths perform reasonably well in all cases of part design.

3. Fractal-based strategies lead to higher formability and reduced spring-back in some cases with lower overall geometric deviation as it engages most material and exploits larger windows for material flow.

Acknowledgements The authors would like to acknowledge the Department of Heavy Industries, Government of India, and Mahindra & Mahindra for funding the project (sanction number: 7(8)/2019-AEI (19310)). The authors would like to acknowledge the Center of Excellence on Materials and Manufacturing for Futuristic Mobility, IIT Madras also, for the support. The authors would also like to acknowledge undergrad students at IIT Madras, Mansha Kochar and Nithin Padiyar for their assistance in data collection.

References

1. Jeswiet J (2005) Asymmetric incremental sheet forming. In: Advanced Materials Research, vol. 6, Trans Tech Publ. pp 35–58
2. Emmens W, van den Boogaard A (2009) An overview of stabilizing deformation mechanisms in incremental sheet forming. J Mater Process Technol 209(8):3688–3695 https://doi.org/10.1016/j.jmatprotec.2008.10.003. https://www.sciencedirect.com/science/article/pii/S0924013608007267
3. Filice L, Fratini L, Micari F (2002) Analysis of material formability in incremental forming. CIRP Ann 51(1):199–202. https://doi.org/10.1016/S0007-8506(07)61499-1 https://www.sciencedirect.com/science/article/pii/S0007850607614991
4. Bhattacharya A, Maneesh A, Venkata Reddy N, Cao J (2011) Formability and surface finish studies in single point incremental forming
5. Ambrogio G, Gagliardi F, Bruschi S, Filice L (2013) On the high-speed single point incremental forming of titanium alloys. CIRP Annals 62(1):243–246
6. Vanhove H, Mohammadi A, Guo YS, Duflou JR (2014) High-speed single point incremental forming of an automotive aluminium alloy. Key Eng Mater 622:433–439
7. Silva MB, Nielsen PS, Bay N, Cao Martins PAF (2011) Formability and surface finish studies in single point incremental forming. Int J Adv Manuf Technol
8. Ziran X, Gao L, Hussain G, Cui Z (2010) The performance of flat end and hemispherical end tools in single-point incremental forming. Int J Adv Manuf Technol 46:1113–1118
9. Eyckens P, Van Bael A, Aerens R, Duflou J, Van Houtte P (2008) Small-scale finite element modelling of the plastic deformation zone in the incremental forming process. Int J Mater Forming 1:1159–1162
10. Bahloul R, Arfa H, BelHadjSalah H (2014) A study on optimal design of process parameters in single point incremental forming of sheet metal by combining box-bbehnken design of experiments, response surface methods and genetic algorithms. Int J Adv Manuf Technol 74:163–185
11. Desai BV, Desai KP, Raval HK (2014) Die-less rapid prototyping process: Parametric investigations. Procedia materials science 6:666–673
12. Jeswiet J, Hagan E, Szekeres A (2002) Forming parameters for incremental forming of aluminium alloy sheet metal. Proc Inst Mech Eng B J Eng Manuf 216(10):1367–1371
13. Sarraji W, Hussain J, Ren W-X (2012) Experimental investigations on forming time in negative incremental sheet metal forming process. Mater Manuf Process 27(5):499–506
14. Iseki H (1993) Flexible and incremental sheet metal bulging using a few spherical rollers. Trans Jpn Soc Mech Eng 59:2849
15. Matsubara S (1994) Incremental backward bulge forming of a sheet metal with a hemispherical head tool-a study of a numerical control forming system ii. Journal of the Japan society for technology of plasticity 35(406):1311–1316
16. Araghi BT, Manco G, Bambach M, Hirt G (2009) Investigation into a new hybrid forming process: Incremental sheet forming combined with stretch forming. CIRP Ann 58(1):225–228
17. Malhotra R, Cao J, Ren F, Kiridena V, Cedric Xia Z, Reddy N (2011) Improvement of geometric accuracy in incremental forming by using a squeezing toolpath strategy with two forming tools. J Manuf Sci Eng 133(6)
18. Jeswiet J, Micari F, Hirt G, Bramley A, Duflou J, Allwood J (2005) Asymmetric single point incremental forming of sheet metal. CIRP Ann 54(2):88–114. https://doi.org/10.1016/S0007-8506(07)60021-3 https://www.sciencedirect.com/science/article/pii/S0007850607600213
19. Kim T, Yang D (2000) Improvement of formability for the incremental sheet metal forming process. Int J Mech Sci 42(7):1271–1286
20. Hirt G, Ames J, Bambach M, Kopp R, Kopp R (2004) Forming strategies and process modelling for cnc incremental sheet forming. CIRP Ann 53(1):203–206. https://doi.org/10.1016/S0007-8506(07)60679-9 https://www.sciencedirect.com/science/article/pii/S0007850607606799
21. Young D, Jeswiet J (2004) Wall thickness variations in single-point incremental forming. Proc Institut Mech Eng Part B J Eng Manuf 218(11):1453–1459. https://doi.org/10.1243/0954405042418400
22. Duflou J, Verbert J, Belkassem B, Gu J, Sol H, Henrard C, Habraken A (2008) Process window enhancement for single point incremental forming through multi-step toolpaths. CIRP Ann 57(1):253–256
23. Attanasio A, Ceretti E, Giardini C (2006) Optimization of tool path in two points incremental forming. J Mater Process Technol 177:409–412
24. Bârsan A, Racz S-G, Breaz R, Crenganiş M (2023) Evaluation of the dimensional accuracy through 3d optical scanning in incremental sheet forming. Mater Today Proc. https://doi.org/10.1016/j.matpr.2023.03.175 https://www.sciencedirect.com/science/article/pii/S2214785323012178
25. Lee E (2003) Contour offset approach to spiral toolpath generation with constant scallop height. Comput Aid Des 35(6):511–518. https://doi.org/10.1016/S0010-4485(01)00185-3 https://www.sciencedirect.com/science/article/pii/S0010448501001853
26. Nirala HK, Agrawal A (2017) Fractal Geometry Rooted Incremental Toolpath for Incremental Sheet Forming, J Manuf Sci Eng 140 (2):021005. https://asmedigitalcollection.asme.org/manufacturingscience/article-pdf/140/2/021005/6275186/manu_140_02_021005.pdf, https://doi.org/10.1115/1.4037237
27. Skjoedt M, Hancock MH, Bay N (2007) Creating helical tool paths for single point incremental forming. Key Eng Mater 344:583–590
28. Malhotra R, Reddy NV, Cao J (2010) Automatic 3d spiral toolpath generation for single point incremental forming. J Manuf Sci Eng 132(6)
29. Kopac J, Kampus Z (2005) Incremental sheet metal forming on cnc milling machine-tool. J Mater Process Technol 162–163:622–628. https://doi.org/10.1016/j.jmatprotec.2005.02.160 https://www.sciencedirect.com/science/article/pii/S0924013605000804 (**aMPT/AMME05**)
30. Vanhove H, Gu J, Sol H, Duflou J (2011) Process window extension for incremental forming through optimal work plane rotation. In: Special Edition: 10th International Conference on Technology of Plasticity, ICTP 2011. pp 508–512

31. Lu B, Chen J, Ou H, Cao J (2013) Feature-based tool path generation approach for incremental sheet forming process. J Mater Process Technol 213(7):1221–1233. https://doi.org/10.1016/j.jmatprotec.2013.01.023 https://www.sciencedirect.com/science/article/pii/S092401361300040X
32. Tanaka S (2011) Incremental sheet forming with direction control of path planes, ICTP2011. 503–507
33. Hagan E, Jeswiet J (2003) A review of conventional and modern single-point sheet metal forming methods. Proc. Inst. Mech. Eng. B: J. Eng. Manuf. 217(2):213–225
34. Hu VHG, J, S. H, D. JR, (2011) Process window extension for incremental forming through optimal work plane rotation. Steel Res Int 508–512
35. Tanaka S, Hayakawa G, K, T. Nakamura, (2011) Incremental sheet forming with direction control of path planes. Steel Res Int 503–507
36. Li J, Hu J, Pan J, Geng P (2012) Thickness distribution and design of a multistage process for sheet metal incremental forming. Int J Adv Manuf Technol 62:981–988
37. Wu S, Gao L, Matsuoka Y, Rashed S, Zhao Y, Ma N (2022) Multi-step toolpath approach of improving the dimensional accuracy of a non705 axisymmetric part in incremental sheet forming and its mechanism analysis. J Mech Sci Technol
38. Zhu H, Liu L (2021) Research the cnc incremental forming of straightwall parts based on a virtual auxiliary body. J Mater Process Technol 288. https://doi.org/10.1016/j.jmatprotec.2020.116841 https://www.sciencedirect.com/science/article/pii/S0924013620302557
39. Jung K-S, Yu J-H, Chung W-J, Lee C-W (2020) Tool path design of the counter single point incremental forming process to decrease shape error. Materials 13(21). https://doi.org/10.3390/ma13214719 https://www.mdpi.com/1996-1944/13/21/4719
40. Verbert J, Duflou JR, Lauwers B (2007) Feature based approach for increasing the accuracy of the spif process. Key Eng Mater 344:527–534
41. Formisano A, Durante M, Boccarusso L, Memola F (2022) Capece. A numerical approach to optimize the toolpath strategy for polymers forming, J Mech Sci Technol
42. Gupta AK, Shahare H, Kumar P, Dubey AK, Pustovoytov D, Yu H, Pesin A, Tandon P (2023) Effect of tool path strategy and tooltip profile on geometrical feature and surface quality of al-6061 alloy during deformation machining in bending mode. Adv Mater Process Technol 9(1):297–314. https://doi.org/10.1080/2374068X.2022.2091835
43. Nirala HK, Agrawal A (2022) Adaptive increment based uniform sheet stretching in incremental sheet forming (isf) for curvilinear profiles. J Mater Process Technol 306:117610. https://doi.org/10.1016/j.jmatprotec.2022.117610 https://www.sciencedirect.com/science/article/pii/735S0924013622001224
44. Liu Z, Li Y, Meehan PA (2013) Vertical wall formation and material flow control for incremental sheet forming by revisiting multistage deformation path strategies. Mater Manuf Process 28(5):562–571. https://doi.org/10.1080/10426914.2013.763964
45. Ai S, Long H (2019) A review on material fracture mechanism in incremental sheet forming. Int J Adv Manuf Technol 104. https://doi.org/10.1007/s00170-019-03682-6

Publisher's Note Springer Nature remains neutral with regard to jurisdictional claims in published maps and institutional affiliations.

Springer Nature or its licensor (e.g. a society or other partner) holds exclusive rights to this article under a publishing agreement with the author(s) or other rightsholder(s); author self-archiving of the accepted manuscript version of this article is solely governed by the terms of such publishing agreement and applicable law.